SIMS Relative Sensitivity Factors for Al/Mg in Synthetic and Madagascar Hibonite

G. J. MacPherson[1*], J. Beckett[2], N. T. Kita[3], K. Nagashima[4], A. N. Krot[4], J. Fournelle[5], L. Kööp[6], A. T. Hertwig[7], T. R. Rose[1], and A. M. Davis[6]

[1]Dept. of Mineral Sciences, U. S. National Museum of Natural History, Smithsonian Institution, Washington, DC, USA 20560 (macphers@si.edu)

[2]Division of Geological and Planetary Sciences, California Institute of Technology, Pasadena, CA, USA

[3]WiscSIMS, University of Wisconsin, Madison, WI 53706, USA

[4]School of Ocean, Earth Science and Technology, Hawai'i Institute of Geophysics and Planetology, University of Hawai'i at Mānoa, Honolulu, HI 96822, USA

[5]Department of Geoscience, University of Wisconsin, Madison, WI 53706, USA

[6]Department of the Geophysical Sciences, University of Chicago, Chicago, IL 96822, USA

[7]Institute of Earth Sciences, Heidelberg University, 69120 Heidelberg, Germany

Submitted to: *Chemical Geology* August 1, 2022

*Corresponding author

ABSTRACT

We synthesized three compositions of hibonite, differing in their levels of MgO and TiO_2 that were chosen to cover most of the range of compositions of natural meteoritic hibonite. The goal was to evaluate the appropriateness of the use of terrestrial Madagascar hibonite as a standard in the SIMS analysis of initial $^{26}Al/^{27}Al$ ratios in calcium-aluminum-rich inclusions, and especially its use for the determination of the $^{27}Al/^{24}Mg$ relative sensitivity factor (RSF). Concern exists because of the high levels of FeO and rare earth elements (REE) in the terrestrial mineral relative to meteoritic samples. Our results show that, provided the specific Madagascar hibonite samples in a given lab are carefully characterized in terms of mineral chemistry (including Fe, Th, and REE) *via* electron microprobe analysis, the terrestrial mineral gives RSFs that are within 2% of those determined for the synthetic samples. The $^{27}Al/^{24}Mg$ SIMS/EPMA RSF based on the synthetic hibonite compositions alone is 0.779 ± 0.003; combining all synthetic and Madagascar hibonite analyses yields a RSF of 0.777 ± 0.003. We cannot rule out that RSFs might be somewhat different using different SIMS instruments, or among individual SIMS sessions, so RSFs should be evaluated for each SIMS session by using carefully calibrated hibonite standards.

Key words: hibonite, Al/Mg relative sensitivity factor, SIMS analysis

1. INTRODUCTION

Hibonite ($CaAl_{12}O_{19}$) is a rare mineral on Earth but is common in carbonaceous chondrite meteorites, as individual crystals and in Calcium-Aluminum-rich Inclusions (CAIs). Hibonite is the second (after corundum) major-element-bearing phase predicted to condense out of a high-temperature gas of solar composition (Yoneda and Grossman, 1995). It is very resistant to the aqueous alteration that affected many carbonaceous chondrites (e.g., Brearley and Jones 1998), and it even survives the harsh acid treatments used to separate presolar grains from meteorites (Amari et al., 1994). Its physical durability is such that it faithfully preserves isotopic signatures from the time of its formation at 4.567 Ga, including oxygen and magnesium. Meteoritic hibonite tends to be very fine-grained, rarely exceeding 10-20 μm in any dimension, and isotopic analyses generally are made using secondary ionization mass spectrometry (SIMS; a.k.a. ion microprobe). The chemical composition of CAI hibonite is close to the ideal formula, with the one significant substitution being $Mg + Ti^{4+} \Leftrightarrow 2Al$. Some of the titanium is trivalent (see below), implying formation under highly reducing conditions. Terrestrial hibonite, in contrast, contains weight percent levels of rare earth elements (REE), thorium, and iron, with some of the iron being ferric.

Magnesium isotopes in CAIs are analyzed primarily in order to determine excesses in ^{26}Mg that resulted from *in situ* decay of the short-lived nuclide ^{26}Al ($t_{½}$ = 0.705 My) at the time of CAI formation. The original abundance ratio $^{26}Al/^{27}Al$ that can be calculated from the ^{26}Mg excesses is of great importance because of the implications for early solar system chronology and planetesimal heating.

Terrestrial hibonite from Madagascar (the principal source) is commonly used as a standard for SIMS analysis of magnesium isotopes in CAI hibonite, but there are two potential problems with this standard. First, Madagascar hibonite is chemically heterogeneous even withing individual grains (see below). Second, there is concern that the relative sensitivity factor[1] (RSF) for aluminum relative to magnesium may be different in the terrestrial *vs.* meteoritic hibonites due to their differing compositions. For the highest-precision SIMS analyses possible, elimination of any systematic error due to the use of incorrect RSFs is required. We therefore undertook to synthesize pure hibonite close to meteoritic hibonite in composition, then accurately determine the RSFs for

[1] RSF in this system is defined as $^{27}Al/^{24}Mg_{[SIMS]} / {}^{27}Al/^{24}Mg_{[True]}$, where "True" is the value determined by electron microprobe analysis (corrected for ^{24}Mg/total Mg).

this hibonite over a range of Mg and Ti contents, and finally compare those RSFs with ones determined for Madagascar hibonite.

2. METHODS

2.1 Synthesis of Hibonite

2.1.1 Choice of Compositions

It has long been known (e.g., Allen et al. 1978) that there is a ~1:1 correlation between cations of Mg and Ti in meteoritic hibonite, which strongly suggests a charge balanced substitution of $Mg^{2+} + Ti^{4+} = 2Al^{3+}$. Allen et al.'s (1978) assessment utilized 18 hibonite analyses. Figure 1, which shows cations (per 19 oxygens) of Mg *vs.* Ti for 389 hibonite analyses drawn from the literature, displays the same fundamental feature. The vast majority of hibonite analyses adhere closely to a 1:1 line. There is little evidence in Figure 1 for Ti in excess of Mg, but the presence of Ti^{3+} was postulated by Ihinger and Stolper (1986) as the cause of the blue color characteristic of much meteoritic hibonite. Ti^{3+} has since been directly measured in meteoritic hibonite using electron spin resonance (Beckett et al. 1988), electron energy loss spectroscopy (Giannini et al. 2011), and X-ray absorption near edge structure (Doyle et al. 2011).

The compositions of our synthetic hibonites were chosen to cover a range of observed natural compositions, which can be well-described in terms of two endmembers, pure $CaAl_{12}O_{19}$ (Hib) and magnesium-titanium-hibonite ($CaMgTiAl_{10}O_{19}$; MTH). Figure 2 is a histogram of cations of Ti in meteoritic hibonite, illustrating a wide range of compositions up to ~ 0.8 Ti per 19 oxygens (see On-line Supplement 1 for data table and literature references). There is a well-defined peak centered near Ti ~ 0.15, and a broad peak centered on Ti ~ 0.5. Accordingly, we synthesized three compositions corresponding to those two compositions plus an intermediate one of Ti ~ 0.3. All three lie exactly on the binary Hib-MTH and are designated MTH15, MTH30, and MTH50. These bound most of the natural range in Ti contents and provide a basis for interpolation and extrapolation of relationships between the properties of hibonite and their compositions.

The Hib-MTH binary does not completely describe the compositions of natural meteoritic hibonite. First, it is well established that natural blue hibonite contains 10-30% Ti^{3+} (Doyle et al. 2011; Giannini et al. 2011). For our purposes, the role of Ti^{3+} is irrelevant because all our synthetic hibonites were produced under oxidizing conditions (in air); however, this study does not address

the question of whether trivalent titanium might affect the RSF in natural meteoritic hibonite. Second, natural meteoritic hibonite contains minor amounts of Si, V, and Fe. Without a much more extensive collection of precise minor element data, we can only qualitatively assess how close an approximation the Hib-MTH- binary provides for meteoritic compositions. Figure 3 is a histogram of $X_{Hib} + X_{MTH}$, where it is assumed that components involving Si, V, and Fe can be described using one cation in an end-member molecule (e.g., $CaMgSiAl_{10}O_{19}$, $CaV^{3+}Al_{11}O_{19}$, $CaFe^{3+}Al_{11}O_{19}$). To the extent that $X_{Hib} + X_{MTH} < 1$, the other components are significant. Excess Ca, > 1 cation per formula unit, is ignored because this plausibly is a real non-stoichiometric effect (Burns and Burns, 1984; but *cf.* Han et al., 2022). From Figure 3, $X_{Hib} + X_{MTH}$ equals or exceeds 0.9 for 94% of meteoritic hibonites and we conclude that this binary provides a good zeroth order approximation of their compositions. Again however, because our goal is to establish the Al/Mg relative sensitivity factors for hibonite, the role of minor element substitution in natural material can be ignored.

2.1.2 Synthesis Procedures

Samples were synthesized from Alfa Puratronic $CaCO_3$, MgO, Al_2O_3, and TiO_2. The oxides were dried at 400 °C ($CaCO_3$), 800 °C (Al_2O_3, TiO_2), or 1000 °C (MgO) and stored in a vacuum desiccator until weighing. MgO is hygroscopic, so it was weighed first. An amount of MgO approximating the desired weight for a 5 g batch was placed onto the weighing pan of a balance and the oxide allowed to hydrate. The weight was plotted as a function of the square root of time and extrapolated back to zero time (i.e., to the initial anhydrous weight). Weights of the remaining oxides were then adjusted to the weight of MgO to retain the desired stoichiometry. Each oxide mix was ground in an automatic alumina mortar 4½ - 6 hours under ethanol, dried in air, and decarbonated at 800 °C for 65 hours. Decarbonated powder of an oxide mix (~1 gram) was poured into a 13 mm stainless steel pellet die (standard for making KBr pellets). The die was then placed in a hydraulic press, hooked up to a vacuum, and this assembly pressed until an internal pressure of ~19,000 psi was achieved. This was maintained for ~5 minutes. The pressure was then released, the pellet removed and then placed in a Pt cage, suspended using Pt wire, and inserted into the hot spot of a Deltech VT-31 1 atm gas mixing furnace at 1000 ºC in air. The temperature was then increased to 1603 °C at 500 °C /hour and held for 685 hours, followed by a quench through the bottom of the furnace into deionized H_2O. As shown below, the close match between the desired compositions and the resulting run products demonstrates that no loss of magnesium

occurred during synthesis. Also arguing against any loss of magnesium during synthesis is the absence of any modal rutile or other Ti-rich oxide phase. A deficiency of magnesium would have led to excess titanium that could not be incorporated into the hibonite structure by coupled substitution, leading to the formation of such oxides that are not observed.

2.2 Electron Microprobe Analyses (EPMA):

2.2.1 Complicating Factors

Hibonite is structurally more complex than corundum to which it is chemically and cosmochemically similar, containing 6 different cation sites. Burns and Burns (1984) and Bermanec et al. (1996) made detailed structural studies of hibonite, comparing terrestrial and meteoritic varieties. Following the Bermanec et al. model, aluminum occurs in two different 6-fold oxygen-coordinated sites, calcium occupies a 12-fold site, magnesium occupies a spinel-like tetrahedral site, and silicon and Ti^{4+} occupy another 6-fold site. Both Burns and Burns (1984) and Bermanec et al. (1996) speculated that any Ti^{3+} resides in a 5-fold site. Most importantly for present purposes, Mg and Al are light elements whose spectrometer positions (wavelengths) during wavelength dispersive analysis (WDS) vary according to crystallographic site and oxygen coordination numbers. Peak positions for standards and unknowns may not be the same, making precise electron microprobe analysis of hibonite somewhat tricky. This can be ameliorated by using wide slit widths or by analyzing standards and unknowns at their own separate wavelengths. The latter method was employed at the University of Wisconsin and at the Smithsonian, where the most detailed and thorough EPMA analyses were made.

Whereas the composition of meteoritic hibonite can be well defined by the Hib-MTH-binary, Madagascar hibonite contains weight-percent levels of iron oxide (both ferrous and ferric) and REE, and it is very heterogeneous (details given below). The analytical problem is that, if the REE are not explicitly analyzed during electron microprobe analysis, the matrix correction factors determined for all of the other elements will be in error. For example, this can lead to weight-percent-level errors in Al_2O_3. During this study, REE and thorium analyses of Madagascar hibonite were carried out at the University of Wisconsin (only).

2.2.2 Analytical Protocols

To evaluate the compositions of the synthetic hibonite samples, analyses were carried out on four different instruments: a Cameca SX Five field emission electron microprobe at the University of Wisconsin, JEOL JXA-8500F and JXA-8530F Plus field emission "HyperProbes" at the University of Hawai'i and the Smithsonian Institution, respectively, and a TESCAN LYRA3 field-emission scanning electron microscope with focused ion beam (FE-SEMFIB) equipped with an Oxford Wave-500 wavelength-dispersive spectrometer at the University of Chicago. Analyses of Madagascar hibonite were carried out at the Universities of Hawai'i and Wisconsin, and the Smithsonian. Analyses on all four instruments were carried out at 15 keV acceleration voltage and a range of beam currents up to 30 nA (for minor elements in Madagascar hibonite), using natural and synthetic minerals as calibration standards, and data reduction *via* conventional matrix correction correction procedures. In some cases, standards were analyzed as unknowns before and after every run to evaluate and if necessary correct for any systematic errors. At Wisconsin and the Smithsonian, the magnesium and aluminum peak positions were determined independently for standards and unknowns, and those different positions were used during calibration and analysis respectively.

REE and Th in Madagascar hibonite are not explicitly considered here except insofar as they affect the matrix correction factors used to correctly calculate the abundance of the other elements. This effect really only applies to the Wisconsin sample of Madagascar hibonite, as the Hawai'i sample analyses consistently gave analytical sums close to 99% (implying that Th + REE are minor in abundance). However, the Wisconsin sample contains ~ 2-8 wt. % total REE oxides. Therefore, complete electron microprobe analyses of Madagascar hibonite, including REE, were acquired with a Cameca SX Five microprobe at the University of Wisconsin - Madison Geoscience, using Probe for EPMA software (v.9.2.7). Analytical conditions were 15 kV, 20 nA, and a focused beam. Characteristic X-ray intensities were acquired with off-peak backgrounds and processed with the XPP matrix correction. Reference standards used were NIST K412 glass (Mg, A, Ca), wollastonite (Si), Harvard U. hematite (Fe), and synthetic TiO_2 (Ti). Oak Ridge National Lab REE-phosphate glass standards were used for La, Ce, Pr, and Nd; Th-1 diopside glass (provided by J. Donovan) was used for Th. REE Lα lines were acquired with an LIF crystal, and Th Mα with a PET crystal. Interference corrections were made for Nd on Si, La on Pr and La on Ti. PHA settings were in integral mode, except for Al. Detection limits (2σ) for REE and other minor elements were as follows: SiO_2 0.04 wt. %, La_2O_3 0.51 wt. %, Ce_2O_3 0.53 wt. %, Pr_2O_3 0.49

wt. %, Nd_2O_3 0.33 wt. %, Th_2O_3 0.13 wt. %, FeO 0.07 wt. %. In general, most of the REE abundances exceeded detection limits except for Pr.

2.3 SIMS Analysis of $^{27}Al/^{24}Mg$ ratio

Several locations in each synthetic hibonite standard were selected for SIMS analyses that are 5 μm or larger in size and with relatively constant MgO concentrations at μm scale according to FE-SEM EDS analysis. These areas were then analyzed (as described above) for major elements using the University of Wisconsin-Madison electron microprobe, typically 4-10 times each. After the EPMA analyses (using Probe for EPMA, v.12.1.1), selected locations in MTH15 were marked by using focused ion beam (FIB) at the University of Chicago, because of their finer crystal sizes than those in MTH30 and MTH45, according to the procedure described by Defouilloy et al. (2017).

The raw $^{27}Al/^{24}Mg$ ratios of synthetic hibonite and Madagascar hibonite standards were determined using the University of Wisconsin Cameca IMS 1280. The primary O^- ion beam was set to ~ 3 μm diameter and 60 pA and ^{24}Mg and ^{27}Al were detected using monocollection electron multiplier (EM) and Faraday cup (FC), respectively, by magnetic field scan (5 s for ^{24}Mg and 3 s for ^{27}Al integrations, 20 cycles). Other instrument parameters were similar to those reported in Kööp et al. (2016). SIMS spots were chosen to exactly correspond with selected EPMA spot locations. For MTH15 with FIB marks, the marked locations were identified and adjusted precisely to the center of primary beam positions by obtaining ^{27}Al ion images on mono EM following the procedure similar to those described in Hertwig et al. (2019). The secondary ^{24}Mg and ^{27}Al intensities were 5×10^4 to 2×10^5 cps and ~ 4×10^6 cps, respectively. A single analysis took 11 minutes, which is shorter than typical analyses of meteoritic hibonites (e.g., Kööp et al., 2016). The internal errors (2SE) and reproducibility of raw ($^{27}Al/^{24}Mg$) ratios of Madagascar hibonite were 0.3% (2SE) and 1% (2SD), respectively.

Aluminum-magnesium isotopic ratios in hibonites were also measured with the University of Hawai'i Cameca IMS-1280 SIMS using protocols similar to those in MacPherson et al. (2021). The $^{16}O^-$ primary ion beam of -13 keV and ~60-80 pA was focused to ~5 μm diameter. Secondary $^{24}Mg^+$, $^{25}Mg^+$, and $^{26}Mg^+$ ions were measured with the monocollection EM in peak jumping mode,

and $^{27}Al^{+}$ ions were measured with a multicollection FC, simultaneously with $^{25}Mg^{+}$ measurement. Counting times were 4 sec for $^{24}Mg^{+}$ and 10 sec for others, and the measurements typically consisted of 120 cycles. Entrance and exit slits were set to obtain a mass resolving power (MRP) of ~3700, sufficient to separate interference ions from magnesium-isotope signals. The ^{24}Mg count rate ranged from 4×10^{4} to 2×10^{5} among the synthetic and Madagascar hibonites. After SIMS analyses, three EPMA measurements were made around each SIMS pit and an averaged Al/Mg ratio from the three EPMA measurements was used to calculate a RSF value. The EPMA analyses were ~3 μm away from edges of the SIMS pits.

In both labs, EM gains usually are not calibrated, but in general they usually are within 1% of FC values. Dead time is always corrected and regardless would not make more than a few permil difference.

3. RESULTS

3.1 Description and EPMA Analysis of the Samples

3.1.1 Synthetic Hibonite

Figure 4 shows back-scattered electron (BSE) images of the three synthetic hibonite charges. The ubiquitous presence of plate-like and lath-like (plates seen edge-on) shapes indicate that the samples are entirely crystalline. All contain significant pore space, and rare grains of grossite ($CaAl_4O_7$) are present, but otherwise all three compositions produced remarkably pure hibonite. In all three cases, the grain size is small, typically 10-20 μm, but large enough for SIMS analyses.

The averaged EPMA compositions and associated structural formulae measured in all four labs are given in Table 1. All analyses indicate no Si or Fe to be present in any of the samples, within detection limits, typically 0.02 wt. % SiO_2 and 0.03 wt. % FeO. Figure 5 shows stoichiometry diagrams for all three compositions, of two kinds: Mg *vs.* Ti, and Mg + Ti *vs.* Al, both in terms of cations per 19 oxygens. The theoretical compositions of MTH15, MTH30, and MTH50 are shown for reference in the respective diagrams. The diagonal lines indicate the expected trend for the ideal coupled substitutions Mg:Ti = 1:1 and (Mg + Ti) ↔ 2Al. The results from each of the four analytical labs are indicated separately for comparison, although the charts

248 are dominated by the much larger and more comprehensive data set from the University of
249 Wisconsin. All analyses are close to the expected compositions, with none of the labs being
250 systematically closer to ideal than the others. Mg and Ti plot very close to the expected 1:1
251 correlation line and close to the expected values for each composition. Both the Wisconsin and
252 Smithsonian data show slight deficiencies of Al relative to Mg + Ti in the MTH15 and MTH30
253 samples (Fig. 5); it is not clear if this is real or an analytical artifact.

254 All samples show some variability in composition, indicating slight zoning within
255 individual crystals, but within this degree of variability the overall results demonstrate that the
256 synthesis successfully produced the desired compositions.

257 *3.1.2 Madagascar hibonite*

258 Figure 6 shows BSE images of grains from the standard disks used at the Universities of
259 Hawai'i and Wisconsin. The heterogeneity is evident in both disks from the variation in electron
260 albedo, but especially in the Wisconsin disk. Hibonite crystals generally have the morphology of
261 plates, broad and flat perpendicular to the c-axis and thin and tabular parallel to the c-axis. This is
262 illustrated in Figure 7, which shows a close-up BSE image of two of the grains from the Wisconsin
263 disk. One of the grains is oriented such that the plate is lying flat in the plane of the section, whereas
264 the other is edge-on. The extreme heterogeneity seen in the "edge-on" orientation is to a large
265 degree masked in the face-on orientation. This heterogeneity is not so much in the major rock-
266 forming elements as it is in the REE and thorium.

267 Most Madagascar hibonite analyses were obtained at the University of Wisconsin where,
268 in addition to major and minor elements, La_2O_3, Ce_2O_3, Nd_2O_3, Pr_2O_3, and ThO_2 were
269 quantitatively analyzed. Table 2 gives the mean EPMA composition of the Wisconsin sample of
270 Madagascar hibonite. Because no analyses of very-low-REE Madagascar hibonite were obtained
271 in Wisconsin, several WDS analyses were obtained at the Smithsonian as well as several semi-
272 quantitative analyses obtained by energy-dispersive (EDS) analysis. These were aimed at the
273 darkest regions of the "edge-on" grain shown in Figure 7. The Smithsonian EDS analyses of the
274 low BSE albedo areas showed total REE + Th abundances, ≤1 wt. % (as oxides), significantly
275 lower than any of the Wisconsin analyses (presumably because that particular edge-on grain was
276 not analyzed there). Our quantitative WDS analyses (not including REE or Th) of that same dark-
277 albedo hibonite yielded analytical sums on the order of 99%, confirming both that the low albedo

hibonite contains only minor amounts of REE + Th and also that the non-analysis of REE had only a minor effect on the matrix correction factors. The Wisconsin quantitative data show that REE contents in Madagascar hibonite are inversely correlated with Ca, presumably because they occupy the Ca crystallographic site as suggested by Bermacec et al. (1996). This inverse correlation is shown in Figure 8a. Such a graph provides one means (the other being analytical sums) for estimating the total REE content in EPMA analyses if the REE + Th are not directly analyzed, which in turn provides a means for recalculating the matrix correction factors (by artificially introducing REE contents into the WDS computer) to get more precise analyses of the major elements during EPMA analysis.

Figure 8b is a stoichiometry diagram in which total Mg + Fe + Ti is plotted *vs.* Al, all as cations per 19 oxygens. All iron is calculated as ferrous, although this almost certainly is not the case (Burns and Burns, 1984). Nevertheless, the correlation is strong and demonstrates a coupled substitution similar to that shown by the synthetic hibonites, but in this case iron is involved as well. The other and more important point demonstrated by Figure 8b is that the Wisconsin and Hawai‘i samples of Madagascar hibonite are very different. The Wisconsin sample analyses plot close to the ideal correlation line correlation $M^{2+} + M^{4+} \leftrightarrow 2M^{3+}$, but the Hawai‘i sample analyses do not.

3.2 SIMS analysis and Calculation of Relative Sensitivity Factors

The EPMA $^{27}Al/^{24}Mg$ values for all samples were determined somewhat differently at the University of Wisconsin and the University of Hawai‘i. In Wisconsin, EPMA analyses were collected prior to SIMS analysis, by aiming multiple spots within 10-20 μm areas that were identified as relatively homogeneous in Mg concentrations by University of Chicago WDS analyses. Subsequently, the SIMS analysis spots were aimed to exactly coincide with the EPMA analyses areas. Thus, the two kinds of analysis can be directly compared and graphed on a spot-by-spot basis. Madagascar hibonite was analyzed on a few selected grains that had been previously used because they show relatively homogenous EPMA $^{27}Al/^{24}Mg$ ratios. In Hawai‘i, EPMA analyses were done subsequent to SIMS analysis, around the SIMS spots ~3 μm away from spot edges for both MTH and Madagascar hibonite samples. Average values for each spot were used to calculate RSFs. Because the Hawai‘i Madagascar sample is relatively homogeneous compared

with the Wisconsin sample, calculating the three-point post-SIMS averages is not substantively different from having measured the EPMA values prior to SIMS analysis.

In the section below, all University of Wisconsin data and SIMS spot images are contained in On-line Supplements 2 and 3 respectively. All University of Hawai'i data are contained in Supplement 4.

The RSFs are defined as $(^{27}Al/^{24}Mg)_{SIMS}/(^{27}Al/^{24}Mg)_{EPMA}$, which is equivalent to $(^{24}Mg/^{27}Al)_{EPMA}/(^{24}Mg/^{27}Al)_{SIMS}$. Here, we estimate synthetic hibonite RSF as a slope of the linear regression line of the plot $(^{24}Mg/^{27}Al)_{EPMA}$ against $(^{24}Mg/^{27}Al)_{SIMS}$. In this way, the measured ratios from two instruments are expressed by having the larger and less variable number (^{27}Al) in the denominator and smaller and more variable number (^{24}Mg) in the numerator. Any intercept of the regression line represents a small offset in EPMA analyses relative to SIMS analyses, which are more sensitive to low Mg concentrations than EPMA analyses (detection limits of ~10 ppm versus ~0.01%). Because of the larger offset when plotting $(^{27}Al/^{24}Mg)_{SIMS}$ vs. $(^{27}Al/^{24}Mg)_{EPMA}$ the regression line does not provide the same slope as when plotting $(^{24}Mg/^{27}Al)_{EPMA}$ vs. $(^{24}Mg/^{27}Al)_{SIMS}$. This is illustrated in Supplement 1, using the University of Wisconsin data. We use the $^{24}Mg/^{27}Al$ method throughout. Our method assumes the RSF is constant among three synthetic hibonite crystals because the major oxide compositions change only by a few weight %. The fact that data for the three synthetic hibonites lie along straight lines with near-zero intercepts (Figs. 9a, 10a) supports the idea that hibonite composition has an insignificant effect on RSFs. Finally, regression of any one of the three individual synthetic compositions is nearly meaningless anyway because of the very small range of Al/Mg ratios. As shown below (Fig. 11), our assumption is accurate within about 2-3 %.

All data referred to in the following section is summarized in the Appendices and given in detail in the on-line Supplementary Materials.

The Wisconsin data (Appendix 1) are plotted and shown in Figure 9, for all data combined (Fig. 9a) and for each composition separately (Figs. 9b-e). The dashed correlation line is based on the combined synthetic hibonite compositions only, and was calculated using an Isoplot-R model-1 fit. The individual data points adhere closely to the line, whose slope (the RSF) is 0.785 ± 0.004, with an intercept of $(1.81 \pm 0.98) \times 10^{-4}$, and a MSWD of 1.3. The Madagascar hibonite data plot slightly below the correlation line. The RSF for Madagascar hibonite is estimated to be

0.7738±0.0037 by comparing SIMS measured ($^{27}Al/^{24}Mg$) and EPMA ($^{27}Al/^{24}Mg$) ratios, which is –1.4±0.6% relative to the RSF determined from the synthetic hibonites. The data for the Madagascar and synthetic hibonite were collected during the same SIMS run, and in fact the Madagascar hibonite data were used to bracket the synthetic hibonite data, so this difference likely is not due to any SIMS uncertainties. If all data (including Madagascar hibonite) are used to calculate the slope of the correlation line, the resulting slope (RSF) is only marginally different at 0.782 ± 0.004, an intercept of (2.31±0.96) × 10^{-4}, but with a larger MSWD of 3.0.

The Hawai‘i data (Appendix 2) are shown in Figure 10. Like the Wisconsin data, the Hawai‘i determination for Madagascar hibonite plots slightly below (although within error of) the correlation line defined by the synthetic hibonite. The slope of the correlation line (RSF) using just the synthetic hibonite is 0.779 ± 0.004 with a MSWD of 5.6. Using all data, including Madagascar hibonite, yields an identical slope of 0.779 ± 0.004 and MSWD = 5.3. The larger MSWD factors in the Hawai'i data may be due, among other things, to very small uncertainties in some of the EPMA values for the MTH15 and MTH50 compositions. It is possible that the errors are underestimated.

Combining the Hawai'i and Wisconsin data, the RSF based on the synthetic hibonite compositions only is 0.779 ± 0.003 with MSWD = 7.7. Using both the synthetic hibonite and the Madagascar hibonite data, the resulting RSF is 0.777 ± 0.003 with MSWD = 7.2.

Figure 11 shows the correlation between RSF and Al/Mg ratio. The plotted values are averages of individual RSF determinations for each synthetic compositions and are not based on slopes. The Hawai'i data indicate a resolved ~ 2.5% greater value for the RSF of MTH 15 relative to the other two compositions, whereas the Wisconsin data show no resolved difference. The possibility of RSF being dependent on Al/Mg ratio was raised by Wada et al. (2020), especially for very Mg-poor hibonites in which Wada et al. suggested the possibility that the RSF could be as much as 4% higher than for Mg-rich hibonites. Only the University of Hawai'i data provide some support for this idea; although the Wisconsin data hint as such a correlation, it is not resolved.

Because we do not have independent ICP-MS measurements of the magnesium isotopic compositions of either the synthetic or Madagascar hibonites, we cannot quantitatively evaluate instrumental mass-dependent fractionation or its effects on the relative sensitivity factors.

4. DISCUSSION AND CONCLUSIONS

Our results are broadly similar to those of Wada et al. (2020), who used a comparable instrument (Cameca ims-1280HR) at Hokkaido University. They determined the RSF for Madagascar hibonite to be 0.773 ± 0.008 and that for a natural CAI hibonite to be 0.787 ± 0.011, a difference of about 1-2%. However, their result was based on an average of RSFs determined for individual spots and was calculated as $^{27}Al/^{24}Mg$. Recalculating their data the same way as ours, i.e. as a slope of $^{24}Mg/^{27}Al$ (EPMA) *vs.* $^{24}Mg/^{27}Al$ (SIMS), yields a RSF of 0.767 ± 0.008 for all data (i.e. including Madagascar hibonite).

Kööp et al. (2016) determined a RSF for Madagascar hibonite of approximately 0.754, which is 2.5% lower than the value obtained in this study (Table S1). The difference was likely caused by the longer analyses time in Kööp et al. (2016) than this work (2 hours vs. 11 min). As shown in On-line Supplement 3 Table S4, the $^{27}Al/^{24}Mg$ ratios decrease with time in each analysis.

Figure 12 summarizes our RSF determinations along with those of Kööp et al. (2016) and Wada et al. (2020). Two observations emerge. First, the RSF values for synthetic (this work) and meteoritic hibonites (Wada et al., 2020) are within error of each other and close to 0.78. Second, the determined RSFs for Madagascar hibonite are consistently lower than that for either synthetic or meteoritic hibonite, by about 1-2%. As shown below, the difference this bias may cause in inferred initial $^{26}Al/^{27}Al$ values in natural CAIs is small. We thus find that Madagascar hibonite is an appropriate standard during SIMS analysis of Al-Mg isotopes in meteoritic hibonite. However, in any lab making such measurements, it is necessary to carefully analyze the Madagascar hibonite via EPMA. During such analysis, the REE + Th must either be measured or else estimated in order for the EPMA data reduction procedure to correctly calculate accurate matrix correction factors for the major elements.

The effect of RSF on Al-Mg isotopic measurements is to change the $^{27}Al/^{24}Mg$ value of individual hibonite measurements. Increasing the RSF yields a lower $^{27}Al/^{24}Mg$ value, which in turn leads to a higher slope for a $^{26}Mg/^{24}Mg$ *vs.* $^{27}Al/^{24}Mg$ isochron that is strongly influenced by high Al/Mg hibonites. As an example, Kööp et al. (2016) measured internal isochrons for 8 SHIB (spinel-hibonite) inclusions from the Murchison CM2 chondrite. As noted above, the RSF determined by them for Madagascar hibonite was low by about 2.5%. Had they used an RSF closer to 0.78, their determined isochron slopes would be approximately 1% higher. For an isochron with

a slope of 5×10^{-5}, this amounts to a difference of about 0.05×10^{-5}, which is small and has no impact on the conclusions reached by those authors. Another example is shown in Figure 13, which gives Al-Mg isotopic data for a Fluffy Type A inclusion from Allende (TS25-F1, illustrated in Fig. 1a of MacPherson and Krot, 2014). In this object, the hibonite is the phase with the highest Al/Mg. The unpublished data are from the University of Wisconsin. When collected, the data were calculated using a hibonite RSF of 0.73, as shown in in the top figure. If recalculated using 0.78 (bottom figure), the isochron slope (initial $^{26}Al/^{27}Al$) increases from 4.61×10^{-5} to 4.71×10^{-5}. A 6% increase in the RSF leads to a 1.5% increase in slope for this CAI. Were hibonite not the highest Al/Mg phase, the effect of course would be smaller.

We stress that our measurements were made on identical SIMS instruments. Different instruments and different analytical conditions may yield somewhat different RSFs. Counting times in particular have a significant effect.

5. ACKNOWLEDGEMENTS

We thank Dr. Noriyuki Kawasaki and two anonymous reviewers for helpful and constructive reviews. This work was supported by National Aeronautics and Space Administration (NASA) grants NNX15AH68G (GJM, PI), 80NSSC22K1400 (ANK, PI), and 80NSSC17K0251 and 80NSSC21K0374 (AMD, PI). WiscSIMS is partly supported by National Science Foundation grants EAR03-19230 and EAR13-55590.

COMPETING INTEREST STATEMENT:

The authors declare that they have no competing interests.

REFERENCES

Allen, J.M., Grossman, L., Davis, A.M., and Hutcheon, I.D., 1978. Mineralogy, textures and mode of formation of a hibonite-bearing Allende inclusion. Proc. Lunar Planet. Sci. Conf. 9th, 1209-12-33.

Amari S., Lewis R. S., and Anders E. (1994) Interstellar grains in meteorites: I. Isolation of Sic, graphite, and diamond; size distributions of Sic and graphite. Geochim. Cosmochim. Acta 58: 459–470.

Beckett, J.R., Live, D., Tsay, F.-D., Grossman, L., and Stolper, E., 1988. Ti^{3+} in meteoritic and synthetic hibonite. Geochim. Cosmochim. Acta 52: 1479-1495.

Bermanec, V., Holtstam, D., Sturman, D., Criddle, A.J., Back, M.E., Scavnicar, S., 1996. Nezilovite, a new member of the magnetoplumbite group, and the crystal chemistry of magnetoplumbite and hibonite. Can. Mineral. 34: 1287-1297.

Brearley, A. J., and Jones, R. H. 1998. Chondritic meteorites. In *Planetary Materials* (ed. J. J. Papike) Mineralogical Society of America, Washington, D. C., pp. 1–398.

Burns, R.G., Burns, V.L., 1984. Crystal chemistry of meteoritic hibonites. Proc. Lunar Planet. Sci. Conf. 15th, Jour. Geophys. Res. 89. Supplement: C313-C321.

Curien, H., Guillemin, C., Orcel, J., Sternberg, M., 1956. La hibonite, nouvelle espèce minérale. Comptes Rendus Hebdomadaires des Séances de l'Académie des Sciences, 242: 2845-2847

Defouilloy C., Nakashima D., Joswiak D.J., Brownlee D.E., Tenner T.J., Kita N.T., 2017. Origin of crystalline silicates from Comet 81P/Wild 2: Combined study on their oxygen isotopes and mineral chemistry. Earth Planet. Sci. Lett. 465: 145-154.

Doyle P.M., Berry, A.J., Schofield, P.F., Mosselmans, J.F.W., Smith, A.D., Scholl, A., Young, A.T., 2011. The oxidation state of Ti in synthetic and meteoritic hibonite, with application to early solar nebula processes. Workshop on the Formation of the First Solids in the Solar System, #9034.

Giannini M., Boffa Ballaran T., Langenhorst F., and Bischoff A. 2011. TEM-EELS measurements of titanium oxidation state in hibonites. Workshop on the Formation of the First Solids in the Solar System, #9067.

Grossman L 1972. Condensation in the primitive solar nebula. *Geochimica et Cosmochimica . Acta* **36**: 597–619.

Han J., Ohnishi I., Yasuhara A., and Keller L. P. (2022) Atomic-scale structure and non-stoichiometry of meteoritic hibonite: A transmission electron microscope study. American. Mineralogist **107:** 873–884.

Hertwig, A.T., Kimura, M., Ushikubo, T., Defouilloy, C., Kita, N.T., 2019. The ^{26}Al-^{26}Mg systematics of FeO-rich chondrules from Acfer 094: Two chondrule generations distinct in age and oxygen isotope ratios. Geochim. Cosmochim. Acta 253: 111-126.

Ihinger, P.D., Stolper, E., 1986. The color of meteoritic hibonite: An indicator of oxygen fugacity. Earth Planet. Sci. Lett. 78: 67–79.

Kööp, L., Nakashima, D., Heck, P.R., Kita, N.T., Tenner, T.J., Krot, A.N., Nagashima, K., Park, C., Davis, A.M., 2016. New constraints on the relationship between ^{26}Al and oxygen, calcium, and titanium isotopic variation in the early Solar System from a multielement isotopic study of spinel-hibonite inclusions. Geochim. Cosmochim. Acta 184: 151-172.

MacPherson, G.J. and Krot, A.N., 2014. Distribution of Ca-Fe-silicates in CV3 chondrites: Controls by parent-body compaction. Meteorit. Planet. Sci. 49: 1250–1270.

MacPherson, G.J., Krot, A.N., Nagashima, K., 2021. Al-Mg isotopic study of spinel-rich fine-grained CAIs. Meteorit. Planet. Sci. 55: 2529-2538.

Wada, S., Kawasaki, N., Park, C., Yurimoto, H. 2020. Melilite condensed from an 16O-poor gaseous reservoir: Evidence from a fine-grained Ca-Al-rich inclusion of Northwest Africa 8613. Geochim. Cosmochim. Acta 288: 161-175.

Yoneda, S., Grossman L., 1995. Condensation of $CaO–MgO–Al_2O_3–SiO_2$ liquids from cosmic gases. Geochim. Cosmochim. Acta 59: 3413–3444.

Table 1. Compositions of synthetic hibonites compared with calculated (ideal) equivalents

	MTH15					MTH30					MTH50				
	Ideal	U.H. Avg N=3	U.W. Avg N=50	U.C. Avg N=4	S.I. Avg N=25	Ideal	U.H. Avg N=4	U.W. Avg N=81	U.C. Avg N=8	S.I. Avg N=30	Ideal	U.H. Avg N=8	U.W. Avg N=39	U.C. Avg N=6	S.I. Avg N=26
Al_2O_3	88.95	89.06	88.63	88.22	88.28	86.32	87.09	85.88	86.47	85.55	82.84	83.80	82.81	82.45	82.32
MgO	0.90	0.89	0.92	0.92	0.87	1.80	1.82	1.85	1.88	1.76	2.98	2.93	2.94	2.99	2.83
TiO_2	1.79	1.87	1.80	1.80	1.77	3.56	3.77	3.65	3.66	3.48	5.90	6.09	5.91	5.98	5.78
CaO	8.36	8.35	8.39	8.19	8.40	8.33	8.41	8.37	8.31	8.38	8.28	8.27	8.26	8.13	8.29
Total	100.00	100.17	99.73	99.13	99.36	100.00	101.09	99.75	100.31	99.25	100.00	101.09	99.92	99.54	99.24
	Cations per 19 Oxygens														
Al	11.700	11.695	11.692	11.702	11.692	11.400	11.381	11.376	11.386	11.389	11.000	11.004	11.004	10.996	11.015
Mg	0.150	0.147	0.153	0.154	0.146	0.300	0.301	0.310	0.312	0.297	0.500	0.486	0.494	0.503	0.480
Ti	0.150	0.157	0.151	0.153	0.149	0.300	0.314	0.309	0.307	0.295	0.500	0.510	0.501	0.509	0.494
Ca	1.000	0.997	1.007	0.987	1.011	1.000	0.999	1.008	0.995	1.014	1.000	0.987	0.998	0.986	1.008
Total	13.000	12.996	13.003	12.996	13.003	13.000	12.995	13.003	13.000	13.004	13.000	12.988	12.997	12.994	12.998

U.H. – Univ. of Hawai'i; U.W. – Univ. of Wisconsin; U.C. – Univ. of Chicago; S.I. – Smithsonian Institution.

Table 2. Mean composition of Madagascar Hibonite analyzed at the University of Wisconsin

	Mean [N=77]	Maximum	Minimum
SiO_2	0.58	0.87	0.48
Al_2O_3	78.22	79.08	77.36
FeO	4.31	4.62	3.92
MgO	2.46	2.56	2.30
CaO	6.28	6.83	5.63
TiO_2	4.33	4.98	3.59
La_2O_3	1.62	2.46	0.85
Ce_2O_3	2.26	3.41	1.61
Nd_2O_3	0.33	0.58	b.d.
Pr_2O_3	0.12	0.59	b.d.
ThO_2	0.40	0.71	0.13
TOTAL	100.92		

b.d. – below detection

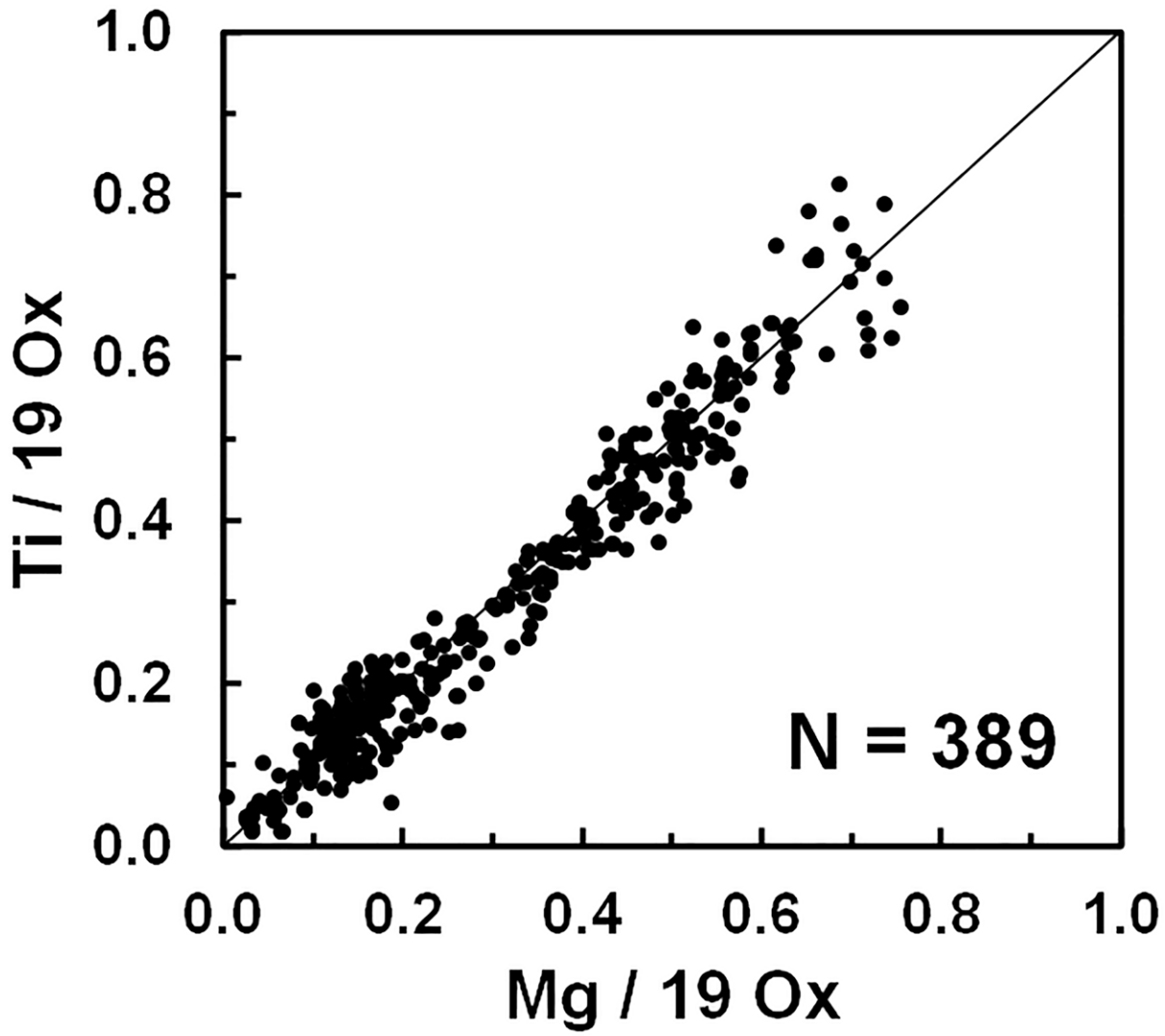

Fig. 1. Cations of Ti per 19 oxygens (calculated as Ti^{4+}) versus cations of Mg in meteoritic hibonite. A 1:1 line is shown for reference. Data are taken from literature; references and data are given in the electronic supplement. Culling criteria are: the nominal oxide total stated by the author(s) agrees with the sum of the oxides ± 0.2 wt.%, the oxide sums are 98-102 wt.%, $SiO_2 \leq$ 1.0 wt. %, Ca cations total 0.96-1.04 per 19 oxygens, and cation sums are 13.00 ± 0.04. The culled data set contains 389 analyses.

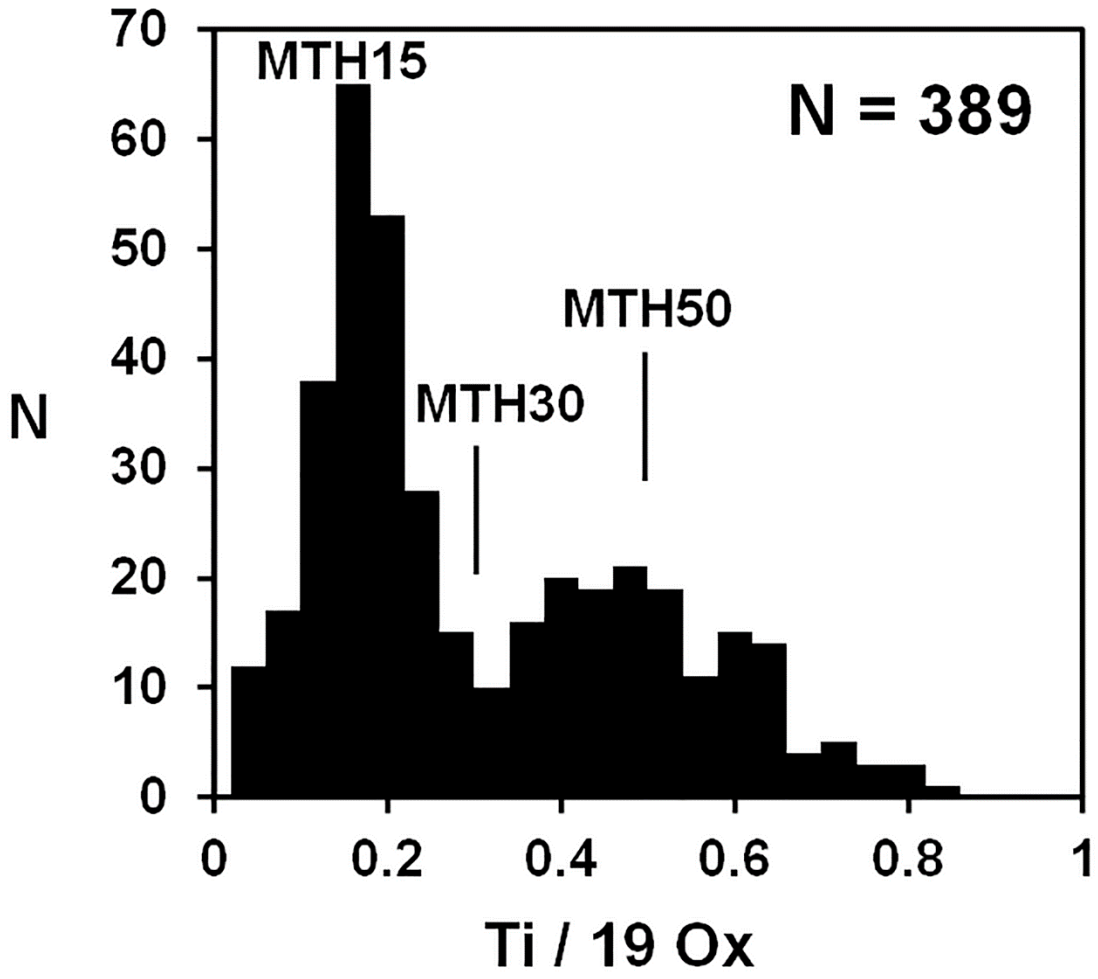

Fig. 2. Histogram of cations of Ti in meteoritic hibonites calculated for a formula with 19 oxygens. Data sources and filtering of analyses as in Fig. 1.

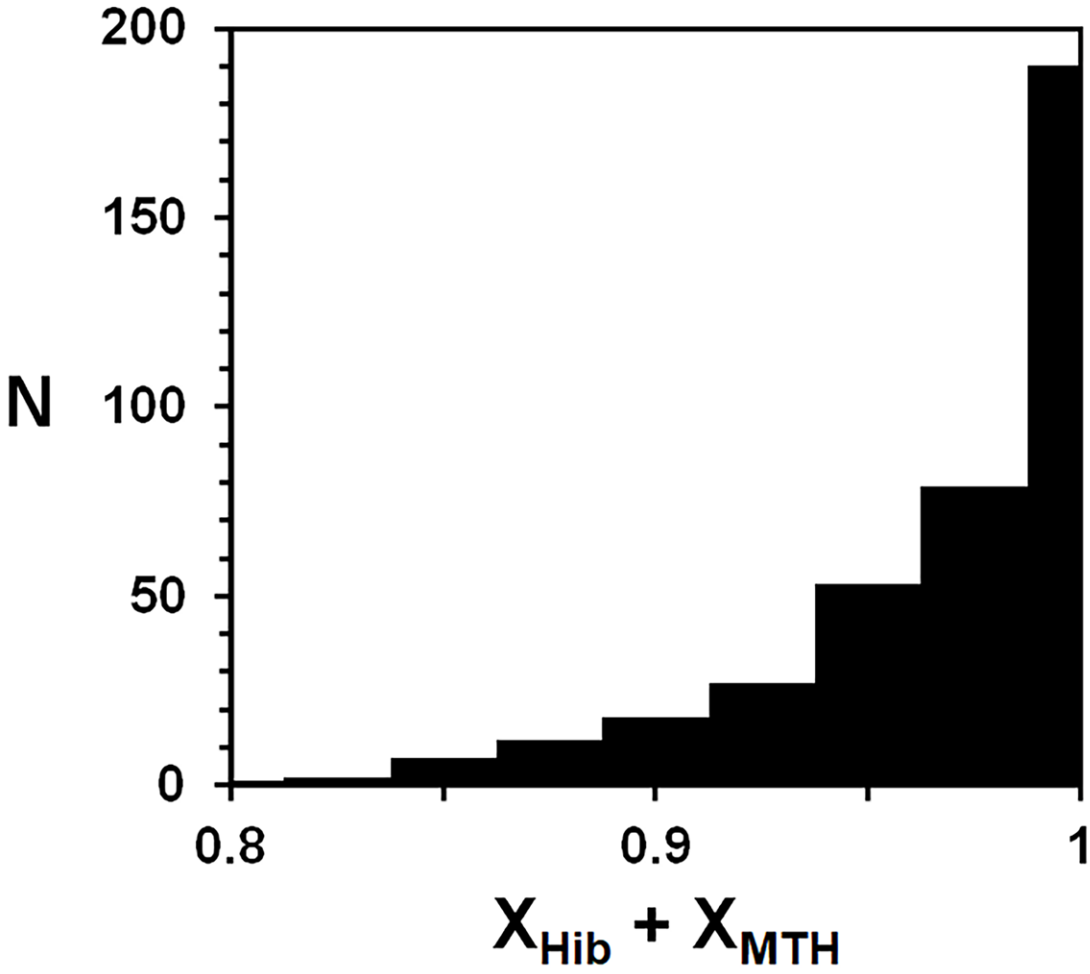

Fig. 3. Histogram of summed hibonite (Hib) + MTH components in natural hibonites. 94% have sums ≥ 0.9, indicating that components such as Si, Fe, and V are minor. Data sources and filtering of analyses as in Fig. 1.

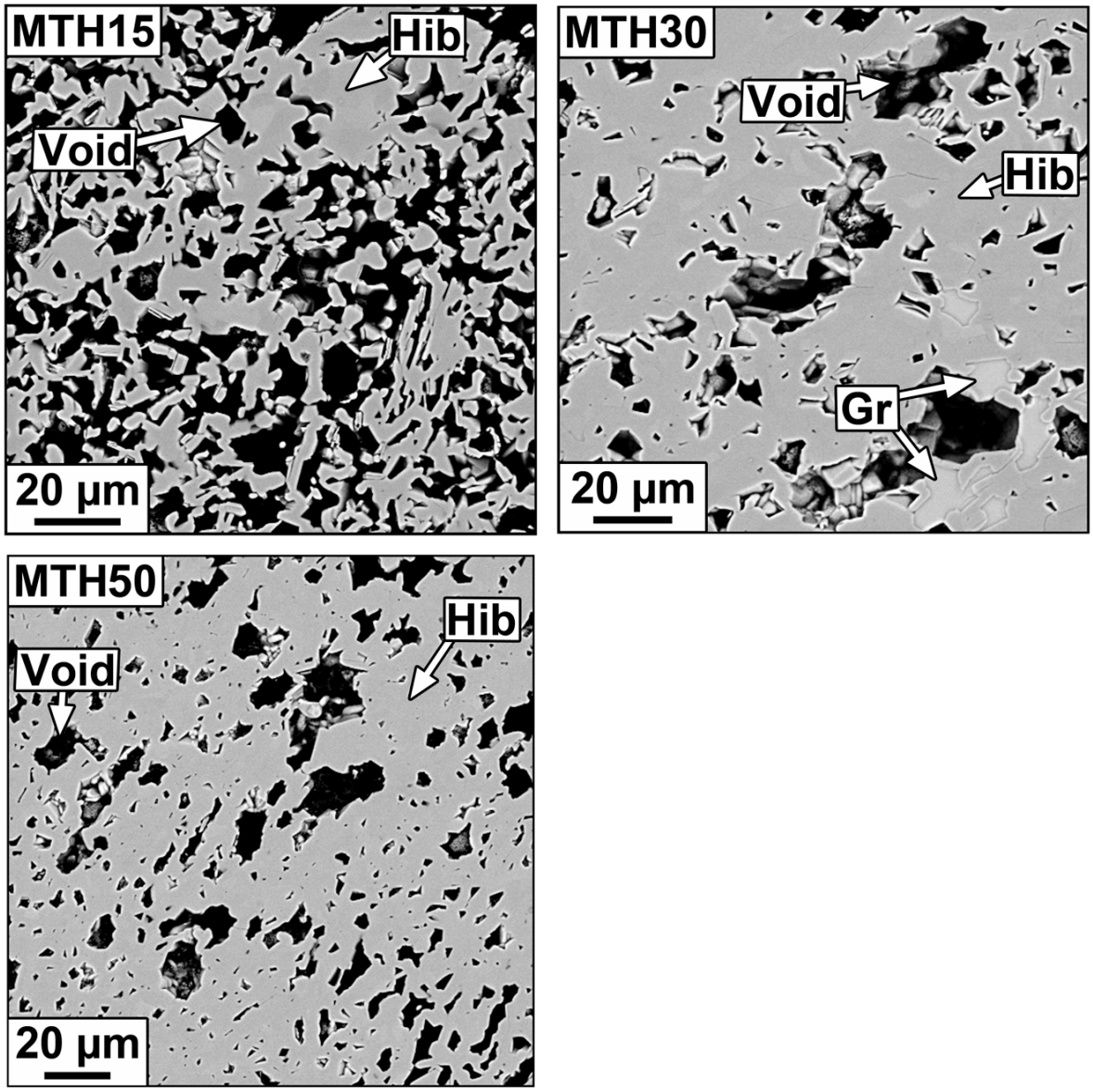

Fig. 4. Back-scattered electron (BSE) images of the three synthesized hibonite (Hib) compositions. Note that well-defined crystal shapes are readily apparent in all three images. Other abbreviations: Gr – grossite

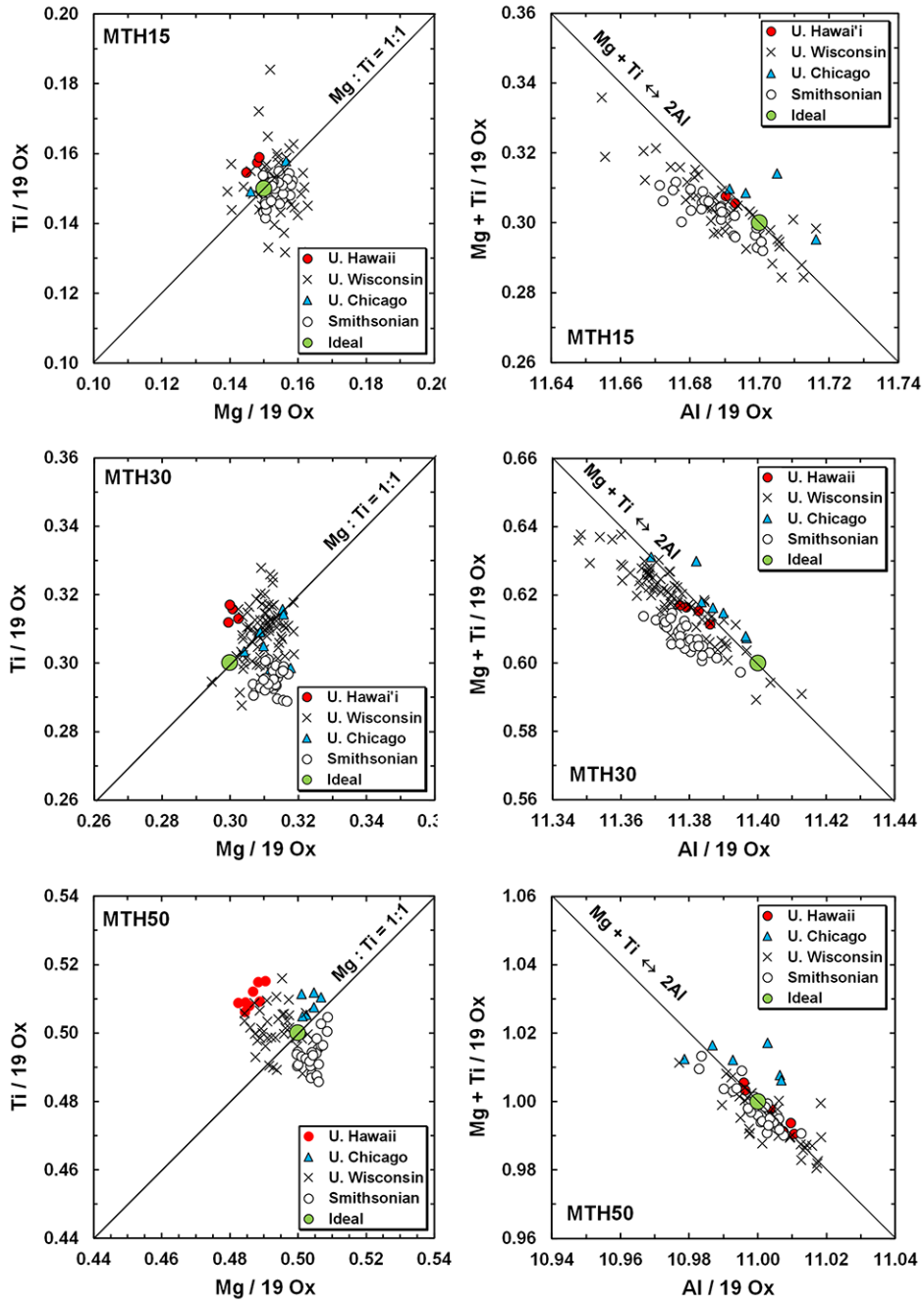

Fig. 5. Stoichiometry diagrams for the three synthesized hibonite compositions, with EPMA data from each of the labs identified.

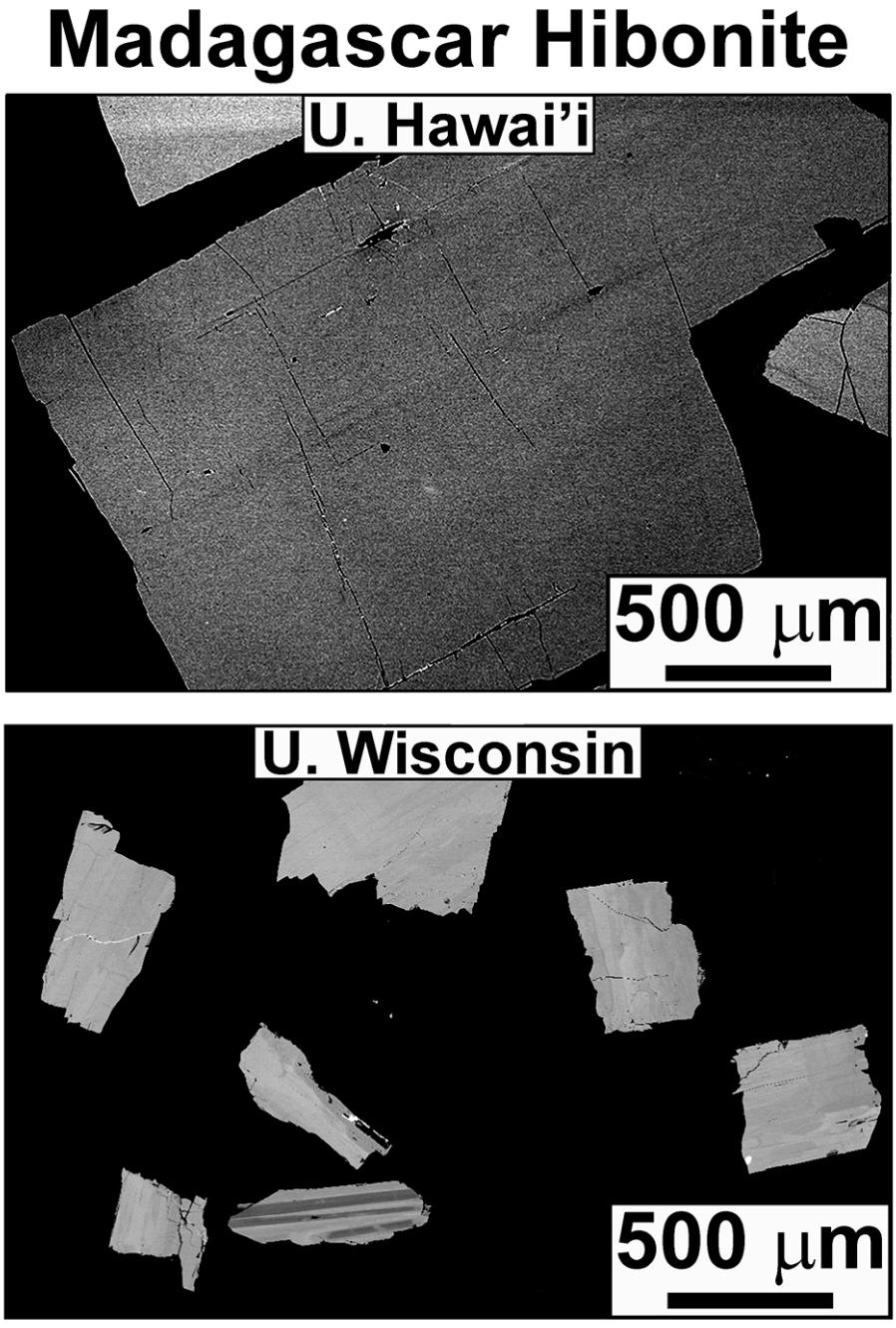

Fig. 6. BSE image of Madagascar hibonite grains in the standard mounts from the University of Hawai'i and University of Wisconsin SIMS labs. The variability in BSE albedo within each image is due primarily to abundance variations in the rare earth elements (REE) and thorium, from < 1 wt. % (total, as oxides) up to ~ 8 wt. %.

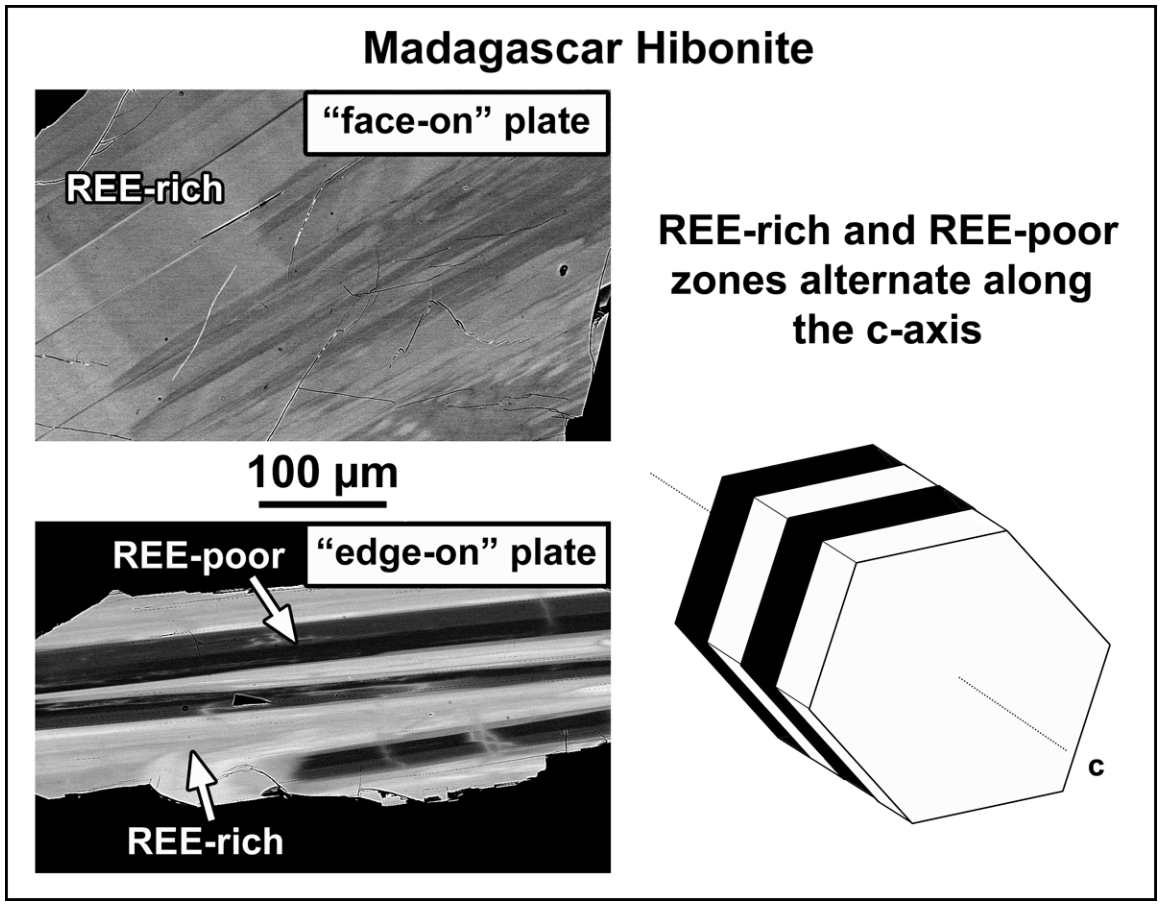

Fig. 7. Enlarged BSE images of two grains of Madagascar hibonite from the UW Standards mount, showing details of the complex zoning patterns. At right is a sketch showing a hibonite crystal with alternating of REE-rich and REE-poor layers. Seen face on, the differing layers are not visible, but seen edge-on the layers are clear.

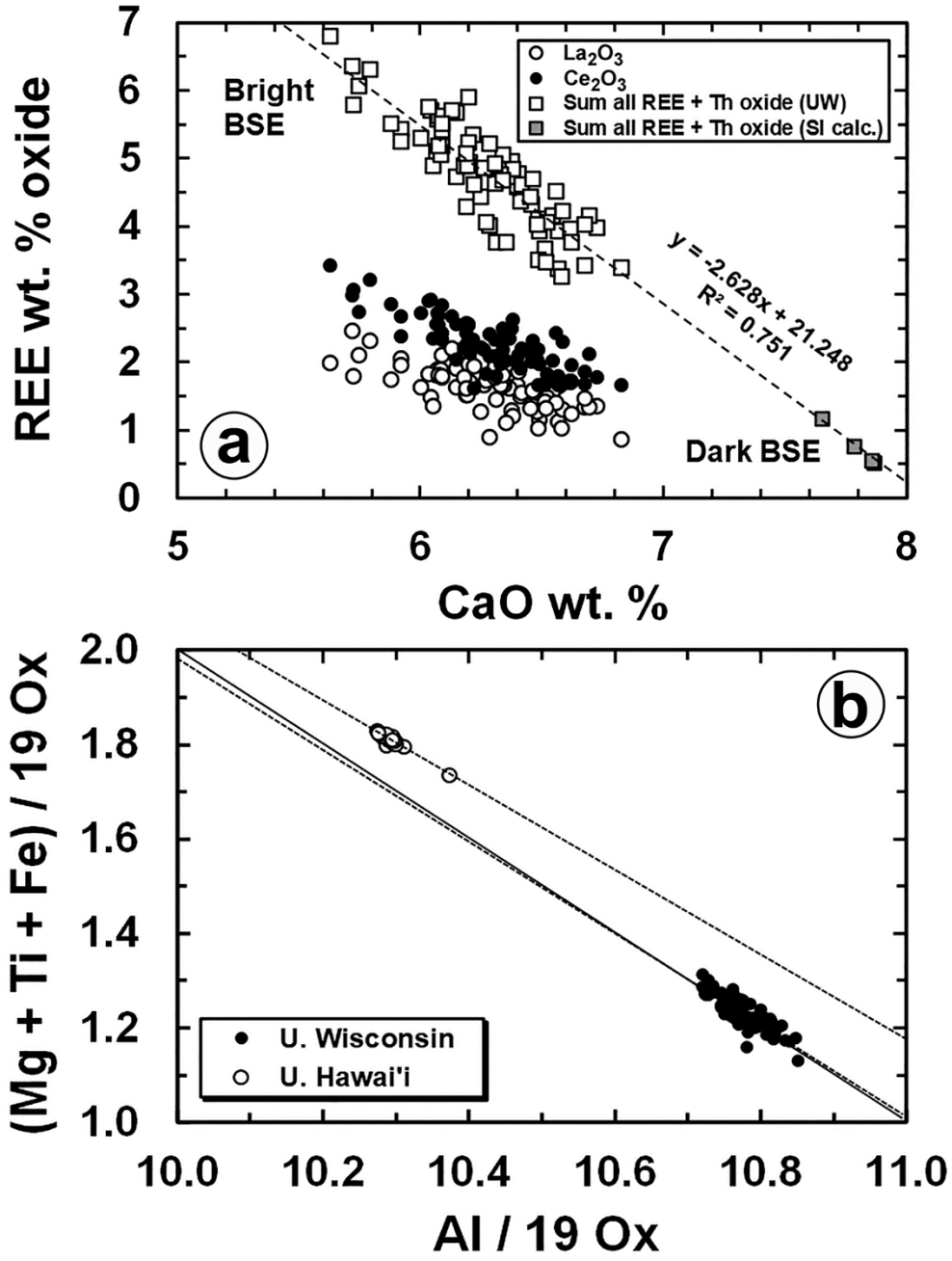

Fig. 8. (a) Plot of weight percent REE + Th oxides vs. CaO in Madagascar hibonite. The inverse correlation indicates that the REE substitute for Ca in the hibonite structure. (b) Plot of total (Mg + Ti + Fe) cations vs. Al cations, all as cations per 19 oxygens. The solid black line marks the ideal correlation $M^{2+} + M^{4+} \leftrightarrow 2M^{3+}$. The dashed lines indicate the best fit correlation line for each data set. The Wisconsin data set closely matches the ideal correlation line (solid line), whereas the Hawai'i data set does not. The Smithsonian data are based on WDS analyses where the total REE + Th was calculated by difference from 100% in the analytical sum.

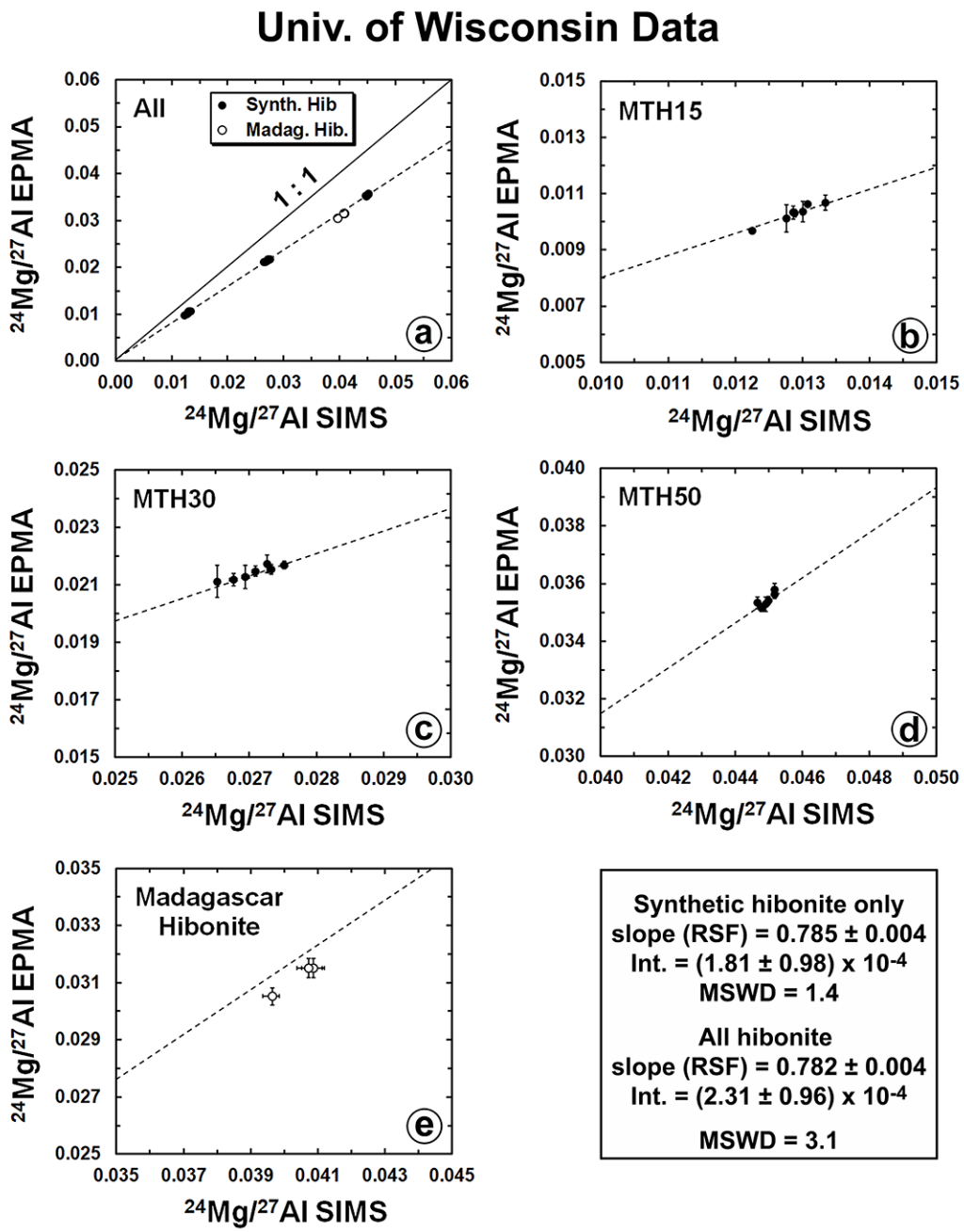

Fig. 9. Plot of EPMA $^{24}Mg/^{27}Al$ vs. SIMS $^{24}Mg/^{27}Al$, using Univ. of Wisconsin data only. The correlation line (dashed) is based on the synthetic hibonite data only. The slope of the correlation line gives the Relative Sensitivity Factor. All errors are 2σ. The solid reference line in (a) marked 1:1 is the expected correlation if the RSF is 1.0. The RSFs given at bottom right are calculated two ways: using only the synthetic hibonite data (upper) and using all data including the Madagascar hibonite data (lower).

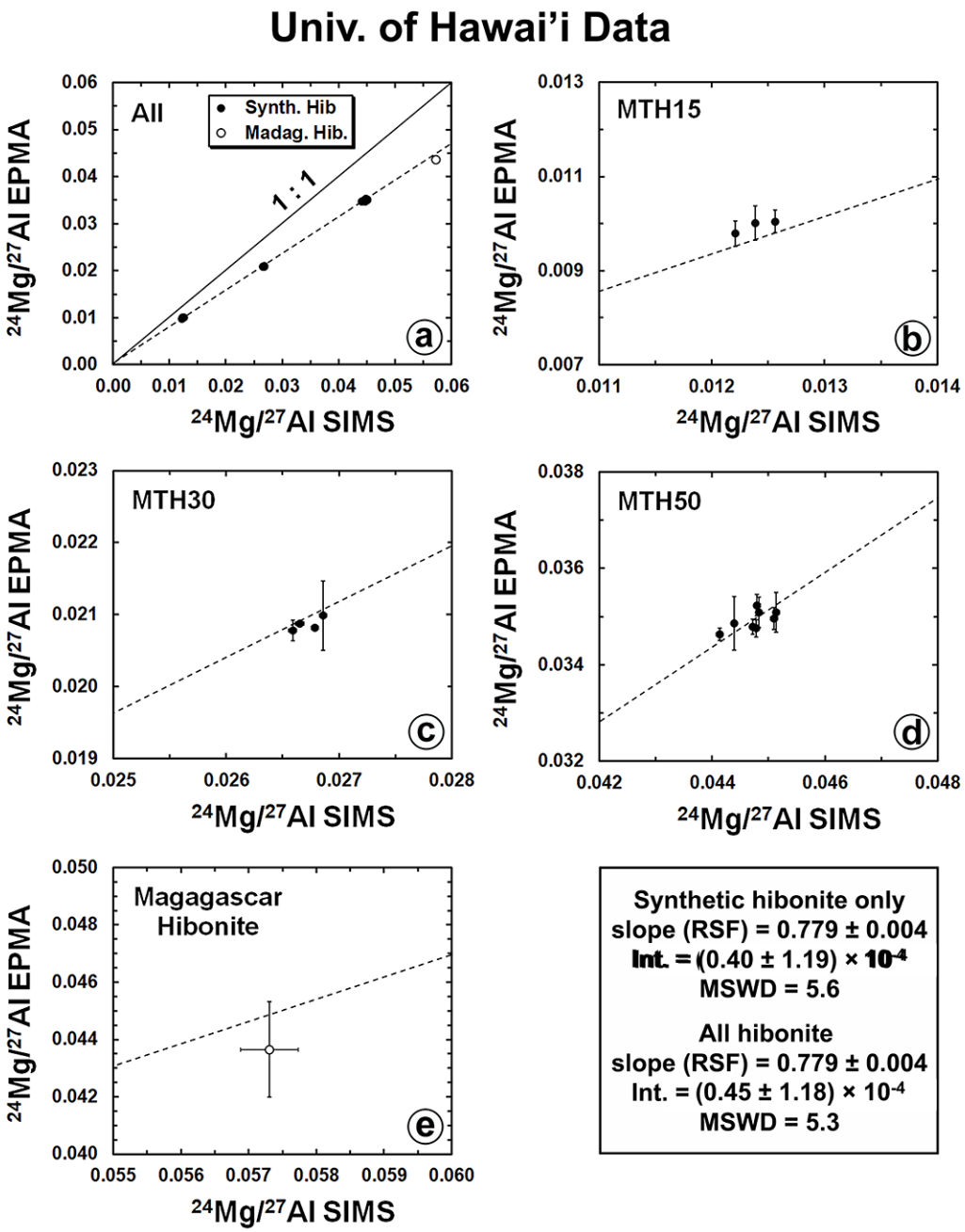

Fig. 10. Plot of EPMA $^{24}Mg/^{27}Al$ vs. SIMS $^{24}Mg/^{27}Al$, using Univ. of Hawai'i data only. All notations as in Fig. 9.

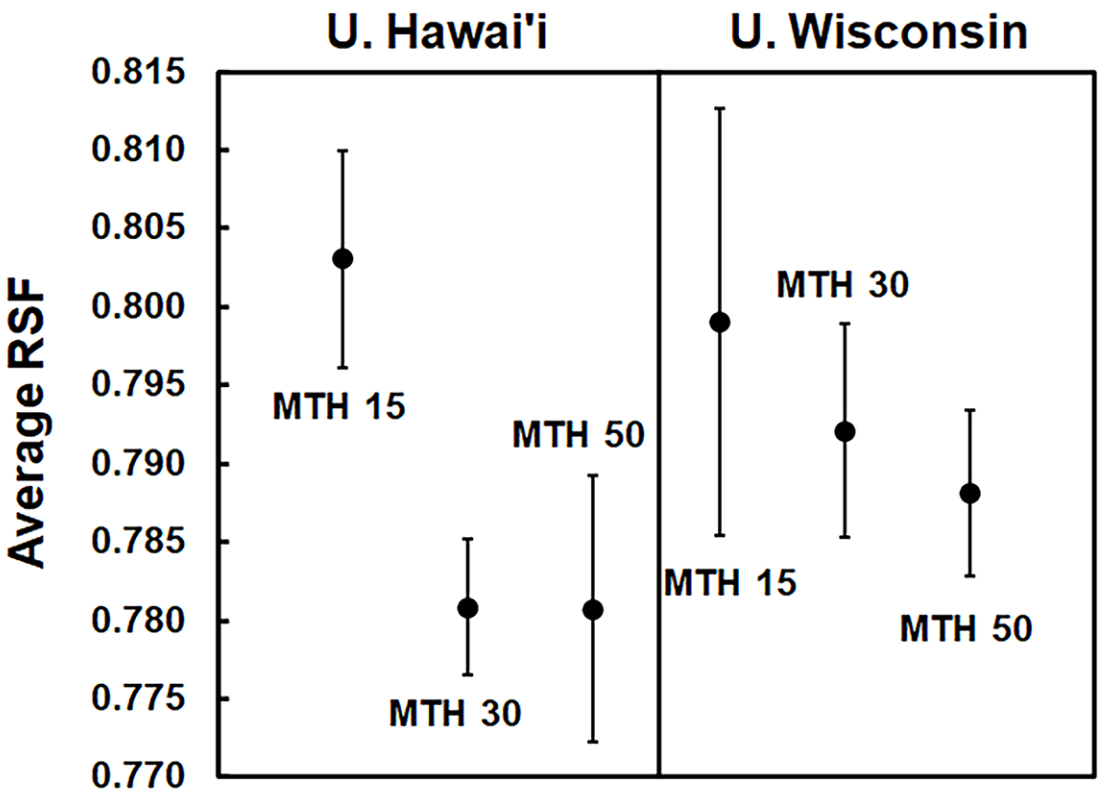

Fig. 11. RSF determinations for individual synthetic hibonite compositions. Values are averages of individual measurements (EPMA/SIMS) and are not based on slopes. Error bars are 2 SE.

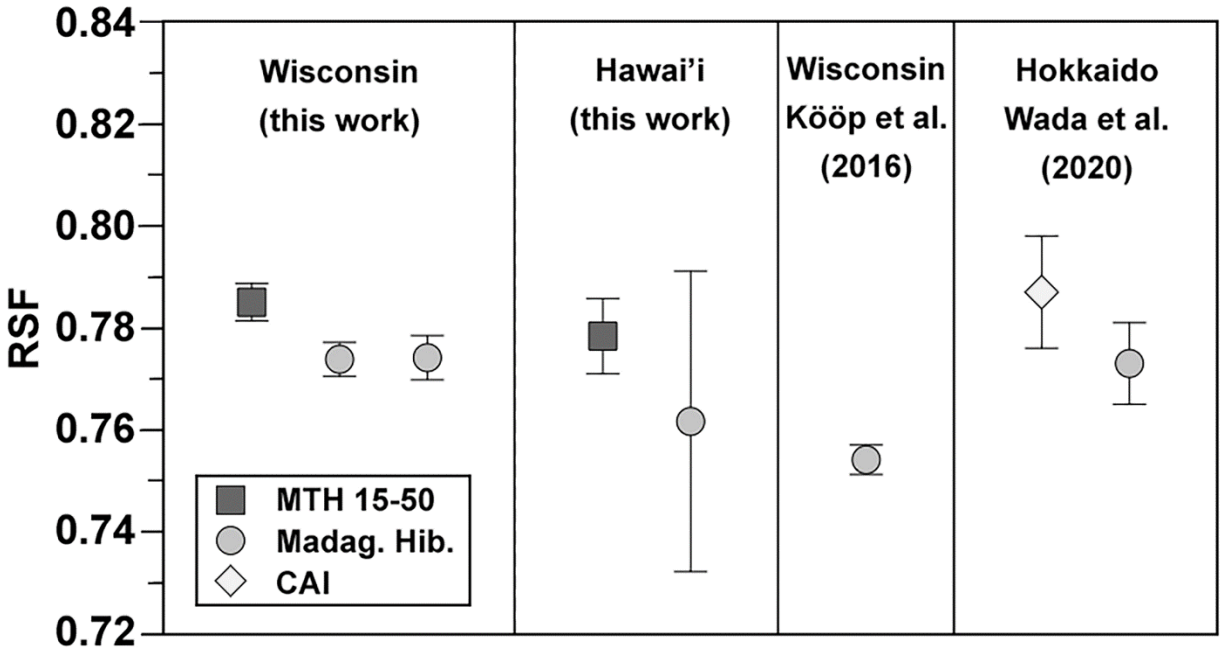

Fig. 12. Summary of hibonite RSF results from this work and from recent literature.

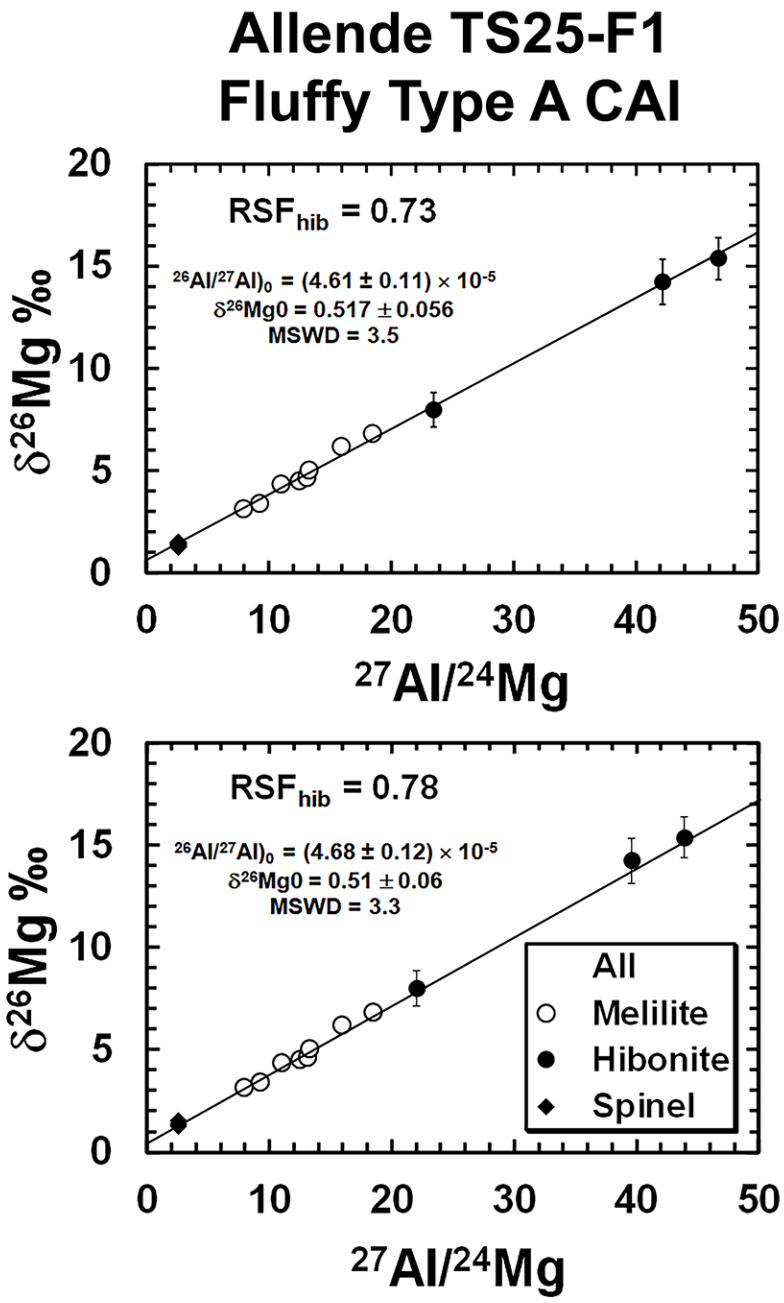

Fig. 13. Plot of $^{27}Al/^{24}Mg$ vs. $\delta^{26}Mg$, for an Allende CAI, showing a 1½% difference in slope caused by a ~6% difference in the RSF used to calculate $^{27}Al/^{24}Mg$. The reason a 6% difference in RSF only leads to a 1.5% difference in slope is in part because there are only three hibonite data points compared to 10 spinel + melilite points, and in part because the hibonite points have larger uncertainties in $\delta^{26}Mg$, so they have less weight in the IsoPlot regression.

Appendix 1: University of Wisconsin summary data

	$^{24}Mg/^{27}Al$ EPMA	$^{24}Mg/^{27}Al$ 2 SE	$^{24}Mg/^{27}Al$ SIMS	$^{24}Mg/^{27}Al$ 2SE	$^{27}Al/^{24}Mg$ EPMA	$^{27}Al/^{24}Mg$ 2SE	$^{27}Al/^{24}Mg$ SIMS	$^{27}Al/^{24}Mg$ 2 SE
MTH15	0.01035	0.00014	0.01301	0.00003	96.66928	1.26500	76.88378	0.46130
MTH15	0.01032	0.00021	0.01286	0.00004	96.92236	1.91548	77.74323	0.46646
MTH15	0.01067	0.00024	0.01335	0.00004	93.76903	2.14680	74.92872	0.44957
MTH15	0.01063	0.00015	0.01308	0.00004	94.10931	1.29895	76.45015	0.45870
MTH15	0.01030	0.00013	0.01288	0.00003	97.09984	1.24188	77.64178	0.46585
MTH15	0.00969	0.00023	0.01225	0.00003	103.32604	2.41243	81.64334	0.48986
MTH15	0.01011	0.00015	0.01276	0.00004	98.91154	1.47982	78.34862	0.47009
MTH30	0.02169	0.00009	0.02752	0.00009	46.10266	0.18333	36.33477	0.21801
MTH30	0.02154	0.00010	0.02732	0.00009	46.42834	0.20969	36.60035	0.21960
MTH30	0.02147	0.00019	0.02709	0.00009	46.57784	0.40946	36.91527	0.22149
MTH30	0.02112	0.00012	0.02652	0.00008	47.35024	0.25690	37.71189	0.22627
MTH30	0.02119	0.00015	0.02676	0.00008	47.19742	0.32158	37.36551	0.22419
MTH30	0.02128	0.00022	0.02694	0.00008	47.00417	0.48832	37.11878	0.22271
MTH30	0.02174	0.00017	0.02727	0.00009	46.00824	0.35356	36.67653	0.22006
MTH50	0.03578	0.00019	0.04518	0.00013	27.94761	0.14485	22.13478	0.13281
MTH50	0.03515	0.00044	0.04478	0.00013	28.45180	0.35025	22.32899	0.13397
MTH50	0.03533	0.00017	0.04466	0.00013	28.30979	0.13586	22.38954	0.13434
MTH50	0.03528	0.00026	0.04491	0.00012	28.34840	0.20489	22.26642	0.13360
MTH50	0.03541	0.00037	0.04500	0.00014	28.24924	0.29747	22.22162	0.13333
MTH50	0.03562	0.00026	0.04518	0.00014	28.08002	0.20694	22.13494	0.13281

Madag. hibonite	0.03052	0.00029	0.03965	0.00020	32.77000	0.31000	25.21878	0.12474
Madag. hibonite	0.03152	0.00034	0.04087	0.00033	31.73000	0.34000	24.46774	0.19550
Madag. hibonite	0.03152	0.00034	0.04073	0.00041	31.73000	0.34000	24.55355	0.24883

RSF Method: $^{24}Mg/^{27}Al$ slope

	RSF	2 SE
(Synth. Only)	0.785	0.004
(All Data)	0.782	0.004

RSF Method: $^{27}Al/^{24}Mg$ slope

	RSF	2 SE
(Synth. Only)	0.800	0.006
(All Data)	0.802	0.006

Appendix 2: University of Hawai'i summary data

	$^{24}Mg/^{27}Al$ EPMA	$^{24}Mg/^{27}Al$ 2SE	$^{24}Mg/^{27}Al$ SIMS	$^{24}Mg/^{27}Al$ 2SE	$^{27}Al/^{24}Mg$ EPMA	$^{27}Al/^{24}Mg$ 2SE	$^{27}Al/^{24}Mg$ SIMS	$^{27}Al/^{24}Mg$ 2SE
	(mean of 3)				(mean of 3)			
MTH15	0.01001	0.00037	0.01239	0.00002	99.96080	3.65746	80.73492	0.10699
MTH15	0.01005	0.00024	0.01256	0.00002	99.56041	2.38754	79.61996	0.10697
MTH15	0.00979	0.00027	0.01221	0.00002	102.19260	2.78661	81.89367	0.10472
MTH30	0.02087	0.00003	0.02665	0.00004	47.90548	0.06192	37.51977	0.05250
MTH30	0.02078	0.00014	0.02659	0.00003	48.12421	0.32246	37.61029	0.04391
MTH30	0.02082	0.00003	0.02679	0.00003	48.02883	0.05827	37.33408	0.04241
MTH30	0.02098	0.00048	0.02686	0.00003	47.65738	1.09418	37.23146	0.03918
MTH50	0.03463	0.00013	0.04413	0.00005	28.87401	0.10926	22.65958	0.02698
MTH50	0.03479	0.00016	0.04472	0.00005	28.74591	0.13158	22.36318	0.02267
MTH50	0.03476	0.00018	0.04478	0.00004	28.77043	0.14801	22.33171	0.02159
MTH50	0.03486	0.00056	0.04440	0.00004	28.68912	0.45914	22.52456	0.01896
MTH50	0.03524	0.00022	0.04480	0.00006	28.37939	0.17480	22.32276	0.02908
MTH50	0.03509	0.00041	0.04514	0.00006	28.50068	0.33576	22.15454	0.02739
MTH50	0.03509	0.00031	0.04483	0.00004	28.50040	0.25417	22.30689	0.02038
MTH50	0.03496	0.00023	0.04510	0.00006	28.60533	0.18439	22.17317	0.02883
	mean of 26		mean of 5		mean of 26		mean of 5	
Madag. hibonite	0.04365	0.00166	0.05731	0.00043	22.91000	0.87000	17.44950	0.13014

RSF Method: $^{24}Mg/^{27}Al$ slope		
	RSF	2SE
(Synth. Only)	0.779	0.004
(All Data)	0.779	0.004

RSF Method: $^{27}Al/^{24}Mg$ slope		
	RSF	2 SE
(Synth. Only)	0.780	0.004
(All Data)	0.780	0.004